# Experimental Study of Hydrophobically Modified Amphiphilic Block Copolymer Micelles Using Light Scattering and Nonradiative Excitation Energy Transfer[†,‡]

**Pavel Matějíček, Filip Uhlík, Zuzana Limpouchová, and Karel Procházka***

*Department of Physical and Macromolecular Chemistry & Laboratory of Specialty Polymers, School of Science, Charles University in Prague, Albertov 6, 128 43 Prague 2, Czech Republic*

**Zdeněk Tuzar**

*Institute of Macromolecular Chemistry, Czech Academy of Sciences, Heyrovský Square 2, 160 00 Prague 6−Petřiny, Czech Republic*

**Stephen E. Webber**

*Department of Chemistry and Biochemistry, University of Texas at Austin, Austin, Texas 78712*

*Received November 28, 2001; Revised Manuscript Received July 30, 2002*

ABSTRACT: The micellization behavior of a hydrophobically modified double tagged polystyrene-*block*-poly(methacrylic acid) diblock copolymer, PS−N-PMA-A was studied in 1,4-dioxane−$H_2O$ mixtures by light-scattering and fluorescence techniques. This polymer was fluorescently tagged by a naphthalene moiety at the junction of the blocks and by anthracene at the end of the PMA block. The behavior of a single-tagged sample, PS−N-PMA, and low-molar-mass analogues were studied for comparison. Multimolecular polymeric micelles with compact PS cores and PMA shells may be prepared indirectly by dialysis from 1,4-dioxane-rich mixtures as water is a strong selective precipitant for the PS block. In both types of micelles, the naphthalene tags are trapped in a nonpolar and fairly viscous core/shell interfacial region. The hydrophobic anthracene tags in PS−N-PMA-A are at the ends of the water-soluble PMA blocks and tend to avoid the bulk polar solvent, burying themselves into the shell. The collapse of a fraction of the PMA chains is an enthalpy-driven process, but it is entropically unfavorable, and the distribution of the anthracene tags in the shell is a result of the enthalpy-to-entropy interplay. Measurements of direct *n*on*r*adiative excitation *e*nergy *t*ransfer (NRET) were performed on PS−N-PMA-A to estimate the distribution of the anthracene-tagged PMA ends in the shell. The experimental fluorometric data show that the anthracene tags penetrate deeply into the shell in water-rich solvents, although there is considerable fluctuation in the distance of closest approach to the excited naphthalene. We find that the collapsed PMA chains and loops in the shell results in the counterintuitive effect that the hydrodynamic radius is significantly increased compared to the corresponding unmodified PS−N-PMA.

## Introduction

In recent years, considerable effort has been devoted to the study of various water-soluble polymeric colloids and nanoparticles. An important member of this class are block copolymer micelles.[1−5] These particles consist of tens to hundreds of hydrophilic/hydrophobic block copolymer molecules and are generally of a spherical shape with tightly packed cores and water-swollen shells. Because of their interesting properties and their potential applications (e.g., in targeted drug delivery, removal of pollutants), water-soluble micelles have been a subject of numerous studies, mainly in the past decade.[6−26] Various micelle-forming block copolymers have been explored which differ in molar mass, glass-transition temperature, polarity of the hydrophobic blocks, and the nature of the hydrophilic blocks.

If the water-insoluble block is only slightly hydrophobic, such as poly(propylene oxide) in Pluronic-type copolymers,[1,3] or is relatively short with respect to hydrophilic block,[9] then the copolymer may dissolve directly in water or aqueous buffers and form equilibrium micelles. Otherwise, micelles must first be prepared in a mixture of water with some organic cosolvent and then transferred into water.[10] Micelles prepared in this way are in a nonequilibrium "frozen" state.[9−11] In our previous work, micelles with polystyrene cores (PS) and poly(methacrylic acid) shells (PMA) have been studied in detail with a special emphasis on fluorescence methods.[27−37] Our preparation method consists of forming PS−PMA micelles in a 20 vol % water/80 vol % 1,4-dioxane mixture followed by transfer into water or aqueous buffers.[28,29] In this 1,4-dioxane-rich mixture, micelles with swollen cores form spontaneously upon dissolution the samples. It has been demonstrated that the structure of a poly(methacrylic acid) shell strongly depends on pH and ionic strength.[30,33−36]

In this paper, we study the structure and behavior of micelles formed by a symmetrical polystyrene-*block*-poly(methacrylic acid) diblock copolymer (PS−PMA) double-tagged by two fluorophores—an excitation energy-donor (naphthalene) located at the $CH_2$−CH(2-Naphth) bridge between the PS and PMA blocks and a fluorescent energy acceptor (anthracene) covalently attached at the free end of the PMA chain. A single tagged copolymer PS−N-PMA was studied for comparison.

* To whom correspondence should be sent. E-mail: prochaz@vivien.natur.cuni.cz

† The study is a part of the long-term research plan of the School of Science, Charles University in Prague, No. MSM 113100001.

‡ Dedication. The authors would like to dedicate the paper to Prof. Petr Munk, Professor Emeritus from the University of Texas at Austin, on the occasion of his 70th birthday.

10.1021/ma012074g CCC: $22.00 
Published on Web 10/29/2002

**Chart 1**

**PS–N–PMA–A**

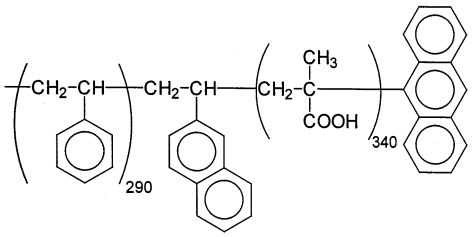


**PS–N–PMA**

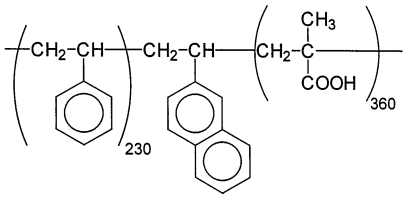


Quasielastic light-scattering measurements together with fluorescence studies of direct *n*on*r*adiative excitation *e*nergy *t*ransfer (NRET) were used for the structural characterization of these micelles, allowing a detailed investigation of their shell structure and determination of the average donor−acceptor distance. Experimental data are interpreted with help of a model developed in the following paper.[39]

## Experimental Section

**Materials. Block Copolymer Samples.** Diblock copolymer samples of polystyrene-*block*-poly(methacrylic acid), (i) a single-tagged sample, PS−N-PMA, with one pendant naphthalene tag between blocks and (ii) a double-tagged sample, PS−N-PMA-A, with one pendant naphthalene tag between blocks and one anthracene tag at the end of the poly(methacrylic acid) block, were prepared by Dr. C. Ramireddy at the University of Texas using anionic polymerization in tetrahydrofuran at −78 °C in a $N_2$ atmosphere, as described earlier.[37,38] (Chart 1). The PS block was prepared first, and then a small amount of 2-vinylnaphthalene (securing an average naphthalene content slightly less than one tag per chain) was added followed by a high excess of *tert*-butyl methacrylate. Adding a very small percentage of the fluorescent comonomer results in a narrow distribution of naphthalene tags in different chains. A small sample of the PS segment was removed and terminated for purposes of characterization by SEC. Termination of the *tert*-butyl methacrylate polymerization was achieved by adding either outgassed $CH_3OH$ in the case of PS−N-PMA or 9-chloromethylanthracene in the case of PS−N-PMA-A which in principle leads to a quantitative tagging of each copolymer chain by one terminal 9-anthryl group. The average content of fluorophores was checked by UV−vis absorption measurements using the extinction coefficients of 2-methylnaphthalene and 9-methylanthracene, and in both cases, there were close to 1.0 tag per chain. The average styrene and methacrylate composition was determined by NMR before removal of the *tert*-butyl group by hydrolysis. The molar mass and polydispersity of the first block and the diblock sample were measured by size-exclusion chromatography using PS standards. The absolute MW of the diblock *tert*-butyl polymer was determined by static light scattering in tetrahydrofuran using the experimentally measured values of the refractive index increment, d$n$/d$c$ = 0.112 (at 633 nm) for both samples. The pertinent experimental values are given in Table 1. The sample was then hydrolyzed by heating with a two-times molar excess of 6 N aqueous HCl (with respect to the PMA) in tetrahydrofuran at 85 °C for 5 h. The dried sample was redissolved in 1,4-dioxane and freeze-dried. The degree of hydrolysis was estimated by NMR and was found to be close to 1.00 (0.98−0.99).

**Table 1. Molecular Characteristics of Polymeric Samples**

| sample | $M_w$/kg·mol$^{-1}$ | $x_{PS}$ | $M_w/M_n$ |
|---|---|---|---|
| PS−PMA | 42.4 | 0.58 | 1.05 |
| PS−N-PMA-A | 60.6 | 0.52 | 1.09 |
| PS−N-PMA | 54.4 | 0.42 | 1.15 |

**Preparation of Polymeric Micelles in Mixed and Aqueous Solutions.** Micellar solutions in 1,4-dioxane−water (20 vol %), which is a mildly selective solvent for PMA, were prepared by direct dissolution of copolymer samples. Solutions with a higher percentage of $H_2O$ were prepared by stepwise dialysis. Finally the solutions of micelles were dialyzed against pure water, exchanging the exterior solvent several times to ensure equilibration.

**Techniques. Static Light Scattering (SLS).** Measurements were performed on a Sofica instrument equipped with a He−Ne laser. Data were treated by the standard Zimm method.[40] Refractive index increments, d$n$/d$c$, were measured on a Brice−Phoenix differential refractometer. When mixed solvents were employed, effective values of $(dn/dc)_\mu$ were measured under the condition of osmotic equilibrium between the solution and the mixed solvent, using a fixed volume dialysis cell.[41]

**Dynamic Light Scattering (DLS).** An ALV 5000 multibit, multitau autocorrelator (Langen, Germany) and an He−Ne laser ($\lambda$ = 633 nm) were employed. The solutions for measurements were filtered through 0.22 $\mu$m Millipore filters. Measurements were performed with solutions of the lowest possible concentration (ca. 0.1 mg/mL) at different angles and temperature of 25 °C. Analysis of the data was performed by fitting the experimentally measured $g_2(t)$, the normalized intensity autocorrelation function, which is related to the electrical field correlation function, $g_1(t)$, by the Siegert relation[7]

$$g_2(t) - 1 = \beta|g_1(t)|^2 \tag{1}$$

where $\beta$ is a factor accounting for deviation from ideal correlation. Two different mathematical procedures were used for evaluation of results. (i) For polydisperse samples, $g_1(t)$ can be written as the inverse Laplace transform (ILT) of the relaxation time distribution, $\tau A(\tau)$:

$$g_1(t) = \int \tau A(\tau) \exp(-t/\tau) \mathrm{d} \ln \tau \tag{2}$$

where $t$ is the lag-time. The relaxation time distribution, $\tau A(\tau)$, is obtained by performing an inverse Laplace transform (ILT) with the aid of a constrained regularization algorithm (REPES),[42] which minimizes the sum of the squared differences between the experimental and calculated $g_2(t)$. The individual mean diffusion coefficients, $D$, are calculated from the second moments of the peaks, where $q = (4\pi n_0/\lambda) \sin(\theta/2)$ is the magnitude of the scattering vector and $\Gamma = 1/\tau$ is the relaxation rate. Here $\theta$ is the scattering angle, $n_0$ the refractive index of pure solvent, and $\lambda$ the wavelength of the incident light.

(ii) The average diffusion coefficient and polydispersity was evaluated using the cumulant method, which employs the relation

$$g_1(t) = \exp[-\Gamma(q)t + \mu_2(q)t^2 + O(t^3)] \tag{3}$$

The average diffusion coefficient may be obtained from the first term as $D = \Gamma/q^2$ and the polydispersity index of the diffusion coefficient distribution, $P_D$, from the second moment of the correlation curve, $P_D = \mu_2(q)/\Gamma(q)^2$. The term $O(t^3)$ is a small error on the order of $t^3$. For the relatively monodisperse micellar systems studied in this work ($P_D \leq 0.1$), both methods yield essentially the same diffusion coefficients $D$. The hydrodynamic radius $R_H$ was evaluated from the diffusion coefficient using the Stokes−Einstein formula. The viscosity and refractive index of 1,4-dioxane−water mixtures (for evaluation of $R_H$ values) were determined experimentally and are given in Table 2.

**Table 2. Viscosity and Refractive Indexes of 1,4-Dioxane−Water Mixtures (for Evaluation of QELS Measurements)**

| $x_{DOX}$ | $\eta$ | $n_D^{20}$ |
|---|---|---|
| 0.0 | 0.890 | 1.331 |
| 0.1 | 1.086 | 1.341 |
| 0.2 | 1.296 | 1.352 |
| 0.4 | 1.760 | 1.372 |
| 0.6 | 2.000 | 1.390 |
| 0.7 | 1.947 | 1.400 |
| 0.8 | 1.730 | 1.407 |
| 0.95 | 1.330 | 1.416 |

**Steady-State Fluorometry.** Steady-state fluorescence spectra (i.e., corrected excitation and emission spectra and steady-state anisotropy) were recorded mainly with a SPEX Fluorolog 3 fluorometer and to a lesser extent with an Aminco Browman, Series 2 fluorometer in 1 cm quartz cuvette closed with a Teflon stopper. Oxygen was removed by 5 min bubbling with nitrogen before the measurement.

**Time-Resolved Fluorometry.** The time-correlated single photon counting technique was used for measurements of fluorescence lifetimes. The time-resolved fluorescence decays were recorded on a ED 299 T time-resolved fluorometer, Edinburgh Instruments, Inc., equipped with a nanosecond coaxial discharge lamp filled with hydrogen at 0.5 atm (half-width of the pulse ca. 1.2 ns).[7] A reconvolution procedure was used to get the true fluorescence decays that were further fitted to multiexponential functions using the Marquardt−Levenberg nonlinear least-squares method using the ED software. Low values of $\chi^2$ (close to 1.0) and random distribution of residuals were used as criteria of the fit.

## Results and Discussion

**Characterization of Micellar Systems in 1,4-Dioxane−Water Solvents by SLS and QELS.** The solutions of single tagged, PS−N-PMA, and double tagged polymeric micelles, PS−N-PMA-A, in a 1,4-dioxane−water (20 vol %) mixture were prepared by direct dissolution of corresponding copolymers in the mixed solvent. The polymer concentration in the mixture in both cases was $5.0 \times 10^{-3}$ g cm$^{-3}$. The 1,4-dioxane-rich mixture is a mild selective solvent for PMA and micelles with swollen PS cores and PMA shells form spontaneously upon dissolution. Solutions in all other solvents, i.e., in 1,4-dioxane with 40, 60, 80, and 100 vol % $H_2O$) were prepared by stepwise dialysis. The exact polymer concentrations in the other micellar solutions were lower and were determined from the volume changes during dialysis.

Molar masses of micelles were measured by static light scattering. The measurements in pure water yield essentially the same particle molar masses, $(M_w)_M$ ca. $8.3 \times 10^6$ g mol$^{-1}$ for PS−N-PMA-A and $7.9 \times 10^6$ g mol$^{-1}$ for PS−N-PMA. This is a reasonable result since both samples have fairly similar unimer molar masses and composition. The former sample contains more PS and therefore its molar mass is slightly higher. Characterization of the micellar sizes (hydrodynamic radius) was performed by QELS. The data showed the presence of only one kind of particle in all solutions, ascribed either to unimers (in the mixture containing 95 vol % 1,4-dioxane) or to fairly monodisperse micelles (in all other mixtures). The polydispersity in micellar sizes, evaluated from the first and second cumulant of the autocorrelation curve, was always lower than 0.1. Figure 1 shows the hydrodynamic radius, $R_H$, of PS−N-PMA micelles (curve 1) and PS−N-PMA-A micelles (curve 2) as a function of the solvent composition. The hydrodynamic radii, $R_H$, increase significantly with increasing water content up to 40 vol % and then slightly decrease until 80 vol % of $H_2O$, for both types of micellar systems. The shape of the curves is basically similar to curves measured earlier for other PS−PMA systems.[28] The hydrodynamic radius is appreciably larger for the double-tagged micelles than for the single-tagged ones, which is surprising for micelles with very similar molar masses and block lengths for the constituent polymers. The physical basis for these size differences is the result of the specific behavior of micelles with hydrophobically modified ends of PMA blocks and will be discussed later, together with the NRET results. It is important to realize that the difference in sizes cannot be due to the difference in micellar masses. The PS−N-PMA-A micelles have slightly higher molar masses, but the main (however not large) difference consists of the lengths of PS blocks. Since the cores are very compact, we may estimate that the difference in core radii cannot exceed 10%. The size of water-soluble micelles is controlled mainly by the shell thickness. The length of shell-forming blocks is similar in both types of micelles and hence, based on simple geometrical considerations, one would expect similar size for both types of micelles.

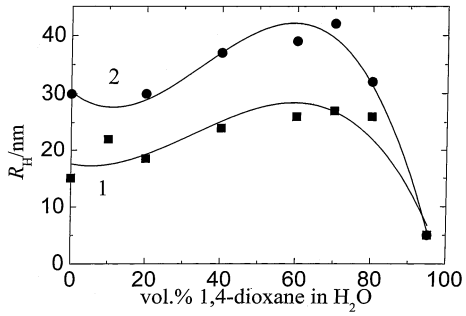


**Figure 1.** Hydrodynamic radii, $R_H$, of polystyrene-*block*-poly(methacrylic acid) micelles formed by the single-tagged PS−N-PMA sample (curve 1) and the double-tagged PS−N-PMA-A sample (curve 2) in 1,4-dioxane−water mixtures.

**Steady-State Spectra.** The double tagged PS−N-PMA-A copolymer allows us to use NRET to study the average distance of the ends of the modified shell-forming PMA block from the core/shell interface. The naphthalene-to-anthracene Förster radius is $R_0 = 2.1$ nm in nonpolar media.[43,44] Both tags have often been used in NRET measurements of the structural characteristics of various polymer systems. Holden and Guillet,[45] Liu and Guillet,[46] and Martin and Webber[47] have proposed and tested several steady-state fluorescence methods that yield correct estimates of distances between naphthalene and anthracene in different polymeric systems.

When the PS−N-PMA and PS−N-PMA-A micelles are formed in water-rich media, all naphthalene tags are expected to be localized in the narrow core/shell interfacial region. Because of the proximity of the PS core the micropolarity of the interface is low and the nondissociated PMA forms fairly compact and fairly hydrophobic inner layer. The formation of the dense inner layer is a result of the specific behavior of PMA, which was observed first in aqueous solutions of linear PMA at low pH.[48−55] Because the strongly hydrophobic anthracene tags prefer to avoid the aqueous medium the anthracene ends of PMA chains will tend to bury themselves in the inner, more hydrophobic part of the shell, fairly close to the naphthalene tags. Because the localization of both tags in the shell may influence their

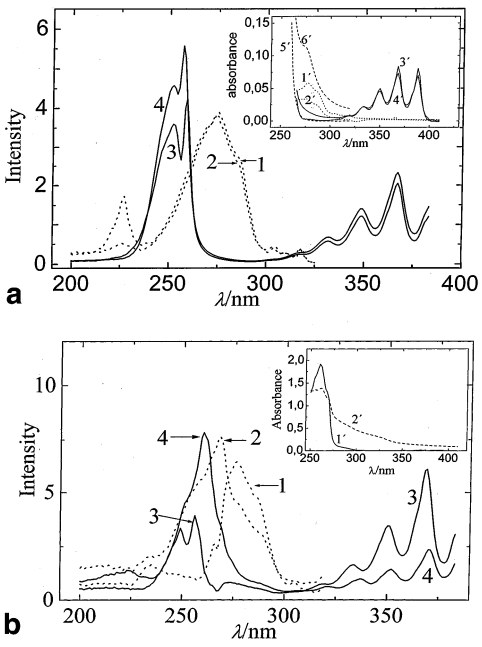


**Figure 2.** (a) Steady-state excitation spectra of low-molar-mass fluorophores in dilute solutions, molar concentration, $c = 1.0 \times 10^{-5}$ mol/L: (i) 2-methylnaphthalene in 1,4-dioxane−water mixtures with 5 and 90 vol % of $H_2O$ (dashed curves 1 and 2, respectively); (ii) (9-anthryl)-3-propionic acid in the same mixtures as before (curves 3 and 4). Inset: Absorption spectra of dilute solutions of low-molar-mass compounds, molar concentration, $c = 1.0 \times 10^{-5}$ mol/L: (i) 2-methynaphthalene in water and in 1,4-dioxane−water mixtures with 5 and 90 vol % of $H_2O$ (curves 1′ and 2′, respectively); (ii) (9-anthryl)-3-propionic acid in the same solvents (curves 3′ and 4′); (iii) blue part of the 9-methylanthracene spectrum in water at two different concentrations, $c = 1 \times 10^{-5}$ mol/L (curve 5′) and $c = 2 \times 10^{-5}$ mol/L (curve 6′). (b) steady-state excitation spectra of fluorescent tags in solutions of polymeric samples: (i) naphthalene tag in the double-tagged PS−N-PMA-A sample in the same solvents (curves 1 and 2); (ii) the anthracene tag in the double-tagged PS−N-PMA-A sample in 1,4-dioxane−water mixtures with 5 and 95 vol % $H_2O$ (curves 3 and 4, respectively), mass concentration of polymers, $c = 1.5$ g/L. Note that the intensity of curves 2 and 4 were reduced by a factor of 2 to make the comparison of the spectra easier (see text). Inset: Absorbance of dilute polymeric solutions of PS−N-PMA-A sample, $c = 1.5$ g/L, in 1,4-dioxane−water mixture with 5 vol % of $H_2O$ (curve 1′) and in water (curve 2′).

quantum yields and spectral properties these effects have to be studied first for low-molar-mass analogues.

Figure 2 shows the steady-state excitation spectra of low-molar-mass compounds. Curves 1 and 2 show spectra of 2-methylnaphthalene (dashed lines) in 1,4-dioxane−water mixtures with 5 and 90 vol % $H_2O$, respectively. Curves 3 and 4 show corresponding spectra of (9-anthryl)-3-propionic acid (full lines). Spectra of 9-methylanthracene are very similar to those of (9-anthryl)-3-propionic acid except that the intensity is lower in media with a large aqueous content (spectra not shown). The short wavelength part of the 2-methylnaphthalene spectrum shows a new band which we assume is due to aggregation in water-rich mixtures. The aggregation behavior of both 2-methylnaphthalene and 9-methylanthracene in water is also apparent from the absorption spectra (inset in Figure 2a). The relative intensity of the 2-methylnaphthalene absorption around 270 nm in water (compare curves 1′ and 2′) and the shoulder in 9-methylanthracene absorption spectrum in water close to 280 nm (the long-dashed curve 6′), increase at higher concentrations, indicating that aggregation is occurring. A comparison of these curves reveals a significant overlap of the 2-methylnaphthalene and the (9-anthryl)-3-propionic acid excitation bands. This demonstrates that the proper choice of the excitation wavelength is very important and may critically influence the accuracy of the energy transfer study.

Figure 2b shows the excitation spectra of the naphthalene tag (dashed curves 1 and 2), the anthracene tag (full curves 3 and 4) in the double-tagged polymer, PS−N-PMA-A in 1,4-dioxane water mixtures with 95 and 5 vol % 1,4-dioxane, respectively. The spectra show very pronounced solvent-dependent shifts. It is necessary to keep in mind that the changes are due to both energy transfer and changes in the viscosity of the microenvironment. While the low-molar-mass fluorophores experience mainly changes in the local polarity as the solvent composition changes, the copolymers form micelles and the fluorophores become embedded in the shell, changing both the local polarity and mobility. As discussed above, we expect the naphthalene tag in PS−N-PMA or PS−N-PMA-A to be located in the fairly rigid core/shell interface. Consequently the fluorescence quantum yield of naphthalene increases dramatically with increasing water content (the fluorescence intensities from micelles in mixtures with 95 vol % $H_2O$ were reduced by a factor of 2 in Figure 2b in order to compare the spectra more easily). The naphthalene excitation spectra in micelles are shifted to longer wavelengths upon the addition of water. In addition to the effect of water on there microenvironment changes, several other factors affect the spectral differences: (i) water is more transparent than 1,4-dioxane in the pertinent spectral region, and (ii) the strong light scattering from micelles in water attenuates the incident light. This fact is apparent from the inset in Figure 2b, which is the absorption spectra of the double-tagged copolymer in 1,4-dioxane-rich and water-rich solvents (curves 1′ and 2′, respectively). The increase in the naphthalene intensity after micellization is smaller for PS−N-PMA-A (curves 3 and 4) than for PS−N-PMA (curves not shown for the sake of simplicity) due to NRET to anthracene. The blue-part of the excitation spectrum of the anthracene tag shows an environment-dependent spectral shift. The observed shift (i.e., a pronounced increase in the excitation between 260 and 275 nm) can arise from a combination of polarity effects and from energy transfer from naphthalene. The environment-dependent shift in the naphthalene excitation maximum position together with the absolute intensity changes indicate that the excitation wavelength has to be chosen properly and all corrections have to be evaluated for individual solutions independently and very carefully (see Appendix). The excitation-dependent emission spectra of the double-tagged micelles in a mild selective aqueous solvent with 80 vol % 1,4-dioxane and pure water are shown in Figure 3, parts a and b, respectively. The emission was scanned from 310 to 500 nm (480 nm in water) for the excitation span from 248 to 296 nm (292 in water). A comparison of these spectra reveals not only the more pronounced NRET effect in water than in the 1,4-dioxane-rich solvent (especially evident for excitation close to 290 nm) but also the strongly increased effect of the direct excitation below 280 nm in water due to the environment-dependent shift of the naphthalene excitation band.

**Evaluation of the Nonradiative Excitation Energy Transfer Efficiency.** For the NRET study, we

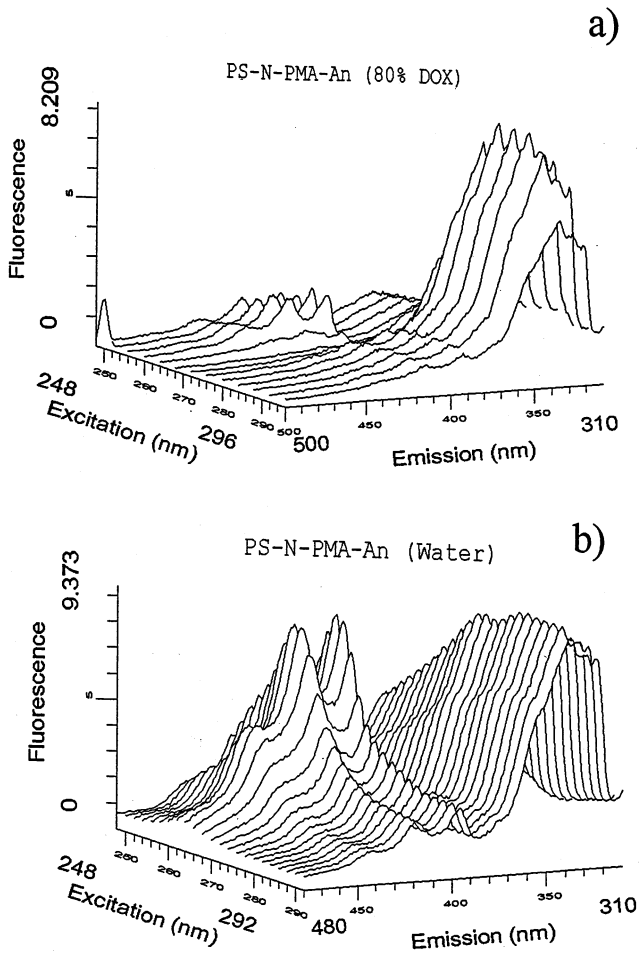


**Figure 3.** Excitation-dependent steady-state fluorescence emission spectra of micellar solutions formed by the PS−N-PMA-A sample in a mild selective 1,4-dioxane−water solvent with 20 vol % $H_2O$ (a) and in water (b). Copolymer concentration in both cases: $c = 1.5$ g/L.

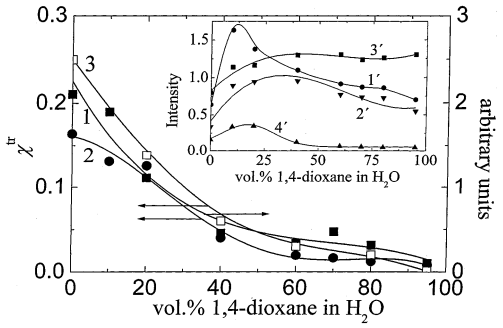


**Figure 4.** Excitation energy transfer efficiency, $\chi^{tr}$, as a function of the solvent composition, $x_{DOX}$. Curve 1: absolute values calculated from the corrected steady-state naphthalene emission spectra of PS−N-PMA and PS−N-PMA-A micelles (using eq 4). Curve 2: relative values based on the corrected sensitized anthracene and quenched naphthalene steady-state emission spectra. Curve 3: absolute values obtained from the time-resolved measurements (using eq 5). Inset: The relative integral fluorescence intensities of tags in polymeric samples as functions of solvent composition. Curve 1: intensity $I^0_D$ of the naphthalene tag in PS−N-PMA sample (unquenched by NRET). Curve 2: quenched intensity $I^q_D$ of the naphthalene tag in PS−N-PMA-A sample. Curve 3: intensity $I^{dir}_T$ of the directly excited anthracene tag (excitation at 380 nm) and curve 4: NRET sensitized intensity $I^{sens}_T$ of anthracene tag (both in PS−N-PMA-A sample). Excited at 275 nm for curves 1, 2, 4.

have chosen the excitation wavelengths $\lambda_D = 275$ nm and $\lambda_T = 370$ nm. The integrated emission from naphthalene (collected in the region from 310 to 450 nm) and anthracene (370−500 nm) are shown in the inset in Figure 4 as functions of the solvent composition. Curve 1 shows the naphthalene intensity in the absence of traps, measured for PS−N-PMA sample (excitation at 275 nm). The naphthalene quantum yield increases with decreasing 1,4-dioxane volume fraction as the naphthalene tags are entrapped in the relatively compact and nonpolar interfacial layer. However, the quantum yield drops by a factor of 2.7 in going from 10% 1,4-dioxane to pure water. We assume this is an environmental effect since the polarity and viscosity of the microenvironment increases considerably after removal of all traces of the preferentially sorbed 1,4-dioxane. There could also be some degree of naphthalene self-quenching as the core−corona interfacial region becomes narrower (see below). Curve 2 shows the NRET-quenched naphthalene emission for PS−N-PMA-A sample, measured under the same conditions and corrected for the concentration of the naphthalene tags. Although $I_D{}^q$ is slightly below $I_D{}^0$, the $I_D{}^q$ curve is parallel to the $I_D{}^0$ curve for > 50% 1,4-dioxane content but starts to decline at 40% 1,4-dioxane. Unlike PS−N-PMA, the fluorescence intensity is essentially constant until 10% 1,4-dioxane and then drops in pure water, with a relative decrease that is a slightly larger than for PS−N-PMA (ca. 3.0 times). Curve 3 shows the directly excited anthracene emission intensity (for the sample PS−N-PMA-A, excitation at 380 nm). There is a relatively smooth decrease for a 1,4-dioxane content below 40%. The sensitized anthracene fluorescence for the same sample is depicted in curve 4 (excited at 275 nm). This intensity increases slightly for a 1,4-dioxane content less than 40% and then drops in pure water. The decrease of the quantum yield in pure water is a general feature of the tagged samples and it has to be taken into account when interpreting the fluorescence behavior. A comparison with the low-molar-mass analogues (see Figure 2a) suggests that the intensity decrease in water-rich media may be partially caused by the aggregation-induced self-quenching of the fluorescence in the shell.

The qualitative features of these intensity changes present a fairly straightforward picture. If the 1,4-dioxane content is high, the average separation of the naphthalene and anthracene moieties in PS−N-PMA-A exceeds $R_0$ (2.1 nm) and NRET is negligible. However, the quantum yield of the naphthalene tag is slightly solvent dependent in the absence of NRET (this holds both for unimers with 95 vol % 1,4-dioxane and for micelles in aqueous mixtures with 40−80 vol % 1,4-dioxane). This is a well-known disadvantage of using naphthalene moieties as fluorescent tags. For a 1,4-dioxane content lower than 40 vol %, the average separation of the naphthalene and anthracene moieties diminishes and NRET becomes much more important. The total spectral response is complex because of the simultaneous changes in quantum yields, spectral shifts of the absorption bands and NRET and as a consequence the evaluation of the NRET efficiency from steady-state spectra has to be done with a great care.

To interpret the steady-state results, we have to recognize that while both samples used in this study are similar, they are not identical, and the same is true of the micelles formed from them. Micellar solutions strongly scatter UV light and as a consequence the experimental absorbance of solutions used for fluores-

cence measurements are high, exceeding 1.0 in pure water. Therefore, even small relative differences are important. The attenuation of the incident light is not equal for both micelle systems and therefore the light absorbed by naphthalene differs. If the measurements are performed for the solutions with the same mass concentrations of both types of micelles, the transfer efficiency, $\chi^{tr}$, may be obtained from the following formula

$$\chi^{tr} = 1 - \frac{(I_D{}^q)_2}{(I_D{}^0)_1} 10^{-\Delta A_{exp}} \left(\frac{c_{T1}}{c_{T2}}\right) \quad (4)$$

where $(I_D{}^0)_1$ and $(I_D{}^q)_2$ are donor (naphthalene) fluorescence intensities from the single-tagged (1) and the double-tagged (2) micellar systems, respectively, $\Delta A_{exp} = A_{exp2} - A_{exp1}$ is the difference in absorbance, and $c_{T1}$ and $c_{T2}$ are molar concentrations of tags in both copolymer samples, respectively (see the Appendix; we note that some terms in eq A1 compensate for each other, but not all of them).

Studying NRET using steady-state fluorescence has the advantage that it allows a simultaneous measurement of the decrease in the donor emission and the concomitant increase in the trap emission. It is possible to express the energy transfer efficiency $\chi^{tr}$ either by the ratio of the sensitized anthracene (trap) fluorescence intensity, $I_T{}^{sens}$, to the quenched naphthalene (donor) fluorescence intensity, $I_D{}^q$, i.e., as$(I_T{}^{sens}/I_D{}^q)$ proportional to $\chi^{tr}(1 - \chi^{tr})$, or by the ratio of the sensitized to direct trap fluorescence intensities, $(I_T{}^{sens}/I_T{}^{dir})$, proportional to $\chi^{tr}$. The evaluation procedure which requires careful corrections is described in the Appendix. We find that evaluation of the transfer efficiency, $\chi^{tr}$, based on formulas containing $I_T{}^{sens}$ is less reliable than that based on the donor emissions only. However, if the excitation wavelength for naphthalene, $\lambda_D$, and anthracene, $\lambda_T$, are well-chosen and all corrections have been properly done, an independent evaluation of the dependence of $\chi^{tr}$ on the solvent composition, i.e., $\chi^{tr} = \chi^{tr}(x_{DOX})$, using the anthracene intensity increases the reliability of the study. The anthracene-derived data can demonstrate if the donor fluorescence quenching in the double-tagged sample is or is not exclusively due to NRET from the donor to traps.

The excitation energy transfer efficiency, $\chi^{tr}$, evaluated from intensities of the nonquenched and quenched naphthalene fluorescence (e.g., using eq 4) is represented by curve 1 in Figure 4, and the relative efficiency, $\chi^{rel}$ scaled to match at 0% dioxane, evaluated on the basis of the properly corrected anthracene emission ratio $(I_T{}^{sens}/I_T{}^{dir})$ is shown by curve 2. It is evident that the trend of the $\chi^{rel}$ curve agrees well with the trend of the absolute $\chi^{tr}$ curve.

**Time-Resolved Fluorescence Measurements.** Time-resolved fluorescence is a suitable experimental technique for the evaluation of the dependence of the energy transfer efficiency on the solvent composition, $\chi^{tr} = \chi^{tr}(x_{DOX})$. The time-resolved data have the advantage that they do not require any complicated correction. Therefore, we believe they are more reliable and more accurate than the steady-state NRET data.

Using the standard methods described in the Experimental section the naphthalene fluorescence decay was fit to

$$I_D(t) = \Sigma_i A_i \exp(-t/\tau_i) \quad (5)$$

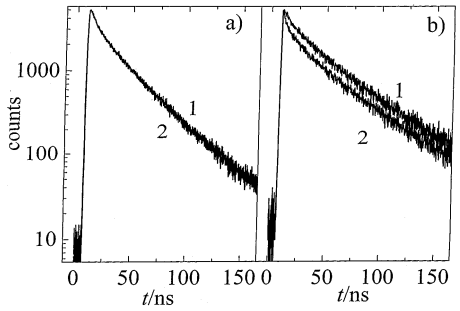


**Figure 5.** Time-resolved fluorescence decay curves: (a) naphthalene tag in PS−N-PMA sample (curve 1) and in PS−N-PMA-A sample (curve 2) in a 1,4-dioxane−water mixture with 5 vol % $H_2O$; (b) naphthalene tag in PS−N-PMA sample (curve 1) and in PS−N-PMA-A sample (curve 2) in 100% $H_2O$. Excited at 275 nm.

where $\tau_i$ represent the lifetime components and $A_i$ are normalized such that their sum is unity. For dynamic quenching by NRET, the transfer efficiency is given by the formula

$$\chi^{tr} = 1 - \frac{\langle \tau_F{}^q \rangle_D}{\langle \tau_F{}^0 \rangle_D} \quad (6)$$

where $\langle \tau_F{}^q \rangle_D$ and $\langle \tau_F{}^0 \rangle_D$ are the mean fluorescence lifetimes of the donor in the presence and in the absence of energy traps, respectively. In this work we use the linear fluorescence lifetime, $\langle \tau_F{}^q \rangle_D{}^{lin} = \sum_i A_i \tau_i$, because it is proportional to the steady-state fluorescence intensity.

The time-resolved naphthalene emission decay curves from the single-tagged and double-tagged polymers in a 1,4-dioxane-rich solvent (5 vol % $H_2O$) are shown in Figure 5a. The decays are not perfectly single-exponential, but both decays essentially superimpose, which suggests that NRET is negligible for PS−N-PMA-A in a solvent that is good for both blocks. The corresponding curves in water are shown in Figure 5b. A comparison of these two curves reveals immediately a strongly nonexponential decay and a considerable shortening of the mean naphthalene fluorescence lifetime in the double-tagged micelles in comparison with the single-tagged micelles. The NRET efficiency, $\chi^{tr}$, evaluated from the time-resolved measurements (curve 3 in Figure 4) agrees fairly well with those obtained from the steady-state measurements. This comparison shows that the properly corrected steady-state data yield also reliable results, although the corrections have to be well understood and performed with care. Note that these corrections may change the raw values by a factor of 2−3.

**The Proposed Structure of the Shell and Distribution of Tags in the Double-Tagged Micelles.** The shell should basically behave as a convex brush formed by an annealed polyelectrolyte.[56] However, PMA also has similarities to a polysoap,[48−55] which significantly modifies the shell behavior. On the basis of our previous studies, it is possible to present the following schematic picture of the shell in unmodified PS−PMA or single-tagged PS−N-PMA micelles in water-rich media (Scheme 1).[32−38] The inner part of the PMA shell (close to the compact PS core) is strongly influenced by low dielectric permittivity of the local environment. The dissociation of carboxylic groups is suppressed, and the PMA forms a fairly compact and hydrophobic layer around the core,

**Scheme 1. Structure of Regular PS−N-PMA Polymeric Micelles (with Nonmodified Shell-Forming PMA Blocks) in Aqueous Media, Including a Schematic Representation of Dependencies of the Density of PMA Segments (Curve 1) and the Degree of Dissociation of COOH Groups (Curve 2) on the Distance from the Core/Shell Interface**

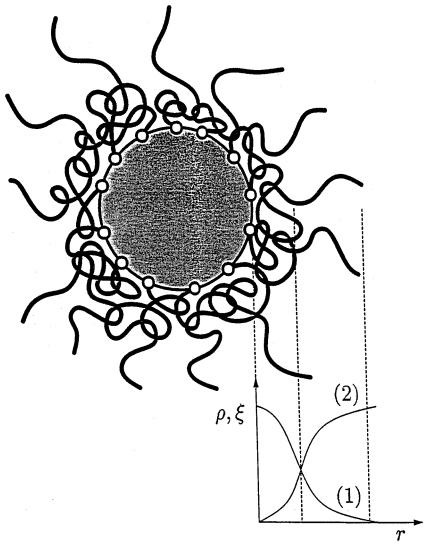


analogous to those in collapsed domains of linear PMA at low pH.[48−55] However the hydrophobicity and density of the inner shell are both considerably higher than linear PMA at low pH and this hydrophobic layer survives up to very high pH.[35,36] The inner PMA layer may solubilize small nonpolar molecules (as does the PS core).[32,33]

The degree of COOH dissociation increases and the segment density decreases in the radial direction from the core toward the shell periphery (see Scheme 1).[56] The ends of PMA blocks in the dilute shell periphery are preferentially stretched in the radial direction due to electrostatic interactions. The overall dissociation and the stretching of dissociated PMA blocks increases with pH, but this effect may be suppressed by the addition of a low-molar-mass salt. Thus, we propose that the shell of high-molar-mass PS−PMA micelles is essentially a two-layer structure. We expect the two-layer character to be very pronounced in micelles with long PMA blocks and diminishes in systems with short PMA blocks.

Experimental data indicate that the shell of the double-tagged PS−N-PMA-A micelles differs appreciably from that described above. Fluorometric decay curves suggest that some anthracene tags are localized fairly deep in the inner shell in water-rich media. The time-resolved naphthalene fluorescence decays of PS−N-PMA-A micelles in aqueous media are strongly quenched at early times, but the rest of the decay (from ca. 30 ns after excitation up to several hundreds of nanoseconds) is unaffected, yielding essentially the fluorescence lifetime of the unquenched naphthalene in PS−N-PMA micelles (see Figure 5b). The peculiar shape of the curve in water, strongly curved at early times but almost parallel with the nonquenched decay at later times, suggests that a relatively small fraction of naphthalene tags is strongly quenched by NRET to anthracene, and the rest are unaffected. Therefore, we assume that there exists a strongly nonuniform and nonrandom spatial distribution of anthracene traps in the micellar shells since only such a distribution may

**Scheme 2. Flower Micelles Formed by ABA Copolymer in a Selective Solvent for B**

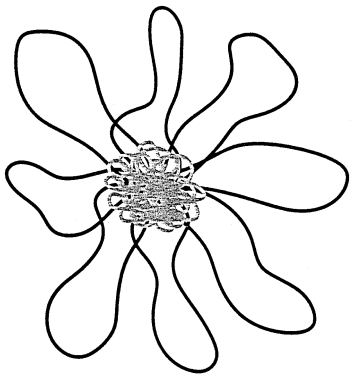

**Scheme 3. Micelles Formed by the Hydrophobically Modified PS−N-PMA-A Copolymer in Aqueous Media**

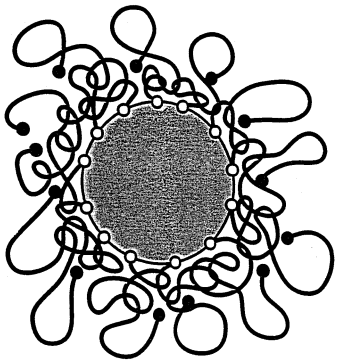

explain the shape of the decay curves. In the following paper, we performe a fairly detailed computer simulation of NRET in model systems in order to analyze this physical system more quantitatively.[39]

Two limiting types of the shell structure have to be considered to rationalize the fluorescence behavior of PS−N-PMA-A micelles: (i) loop-forming PMA chains in the shell and (ii) the shell containing both collapsed and stretched conformations. After some disputes between theoreticians and experimentalists in late eighties,[57,58] the formation of micelles form triblock copolymers ABA with B loops in the shell was reconsidered theoretically and it is now well-recognized.[59] Micelle structures with loop-containing shells were later studied by a number of experimentalists[60−64] and theoreticians (including computer simulations)[65−68] and were named "flower micelles" (Scheme 2). The dual conformation model was proposed theoretically for copolymer brushes under certain conditions.[69]

Our NRET and QELS measurements suggest that the PMA blocks could form relatively loose loops. The chain return is favorable from the enthalpy point of view since the unfavorable anthracene−water interactions are reduced. The formation of loops does not necessarily change the overall degree of carboxylate dissociation compared to regular micelles. Because PMA is an annealed (i.e., weak) polyelectrolyte, the electrical charge can simply move along the loop to the periphery of the shell—see Scheme 3. Obviously the formation of larger loose loops reduces entropy less than the formation of small loops. Therefore, it is reasonable to suppose that a considerable fraction of PMA blocks would form large loops. Taking into account the PMA contour length, there are no steric obstacles that would hinder the formation of micelles with $R_H$ ca. 30−40 nm from PMA loops.

**Scheme 4. Possible Structure of the Shell of Hydrophobically Modified Micelles According to the Mean Field Calculations in Reference 69**

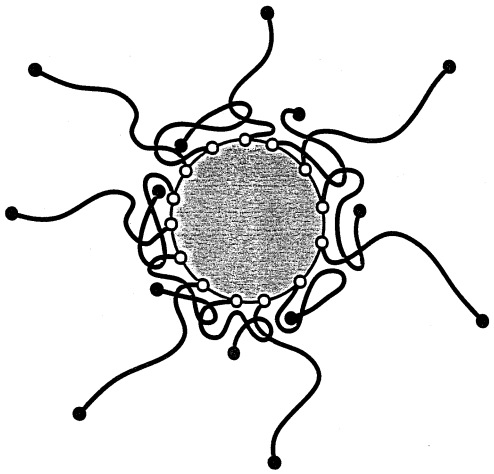

The second conceivable structure, also compatible with the experimental fluorescence decays, is a shell with two types of chains: (i) fully collapsed and (ii) fairly stretched ones. Such a structure would lead to a double-peak radial distribution of traps in the shell—see Scheme 4. So far there is no experimental evidence or support for this type of the shell (in contrast to the experimentally observed flowerlike micelles). Nevertheless, similar structures in copolymer brushes have been proposed by theoreticians on the basis of mean field calculations.[69] For this type of structure, the increased hydrodynamic radius may be also explained by the entropy balance. The reduced entropy of the fully collapsed chains has to be compensated by the increased entropy of the extended ones. Since the entropy of a fully stretched chain is low, an entropy increase may be expected only if there is a relaxation of its tethered part close to the core that normally would be strongly collapsed.

In the following paper, we employ MC calculations to explore more quantitatively the relationship between the distribution of the chain ends and NRET.[39] However, the qualitative results are consistent with the picture presented above. The value of $\chi^{tr}$ and the time dependent fluorescence of the naphthalene can be understood only if the average anthracene−naphthalene separation is in the range 6−2 nm as one goes from 80% dioxane to 100% water. This separation is obviously much smaller than $R_H$ (see Figure 1).

## Concluding Remarks

(1) High-molar-mass hydrophobic/hydrophilic diblock copolymers form spherical multimolecular micelles in aqueous media and aqueous mixtures with suitable organic solvents. In the present work, we have end-capped the hydrophilic block with a hydrophobic fluorophore (anthracene). In contrast to unmodified amphiphilic copolymer micelles, we believe that the hydrophobic tags at the ends of the shell-forming blocks return to the shell interior in order to avoid the aqueous medium, forcing the shell-forming blocks to form loops (see point 4 below). The enthalpy-to-entropy interplay controls the spatial distribution of the modified ends of the shell-forming blocks.

(2) Light-scattering measurements reveal that the formation of PMA loops in water-rich media increased the hydrodynamic radii of double-tagged PS−N-PMA-A micelles as compared with micelles formed by a corresponding single-tagged PS−N-PMA copolymer. On the other hand, the association numbers ($N_{agg}$) of both types of micelles are almost identical since the two polymer samples have quite similar block lengths.

(3) The steady-state and time-resolved measurements of direct nonradiative excitation energy transfer (NRET) between the naphthalene and anthracene allow us to make a reasonable estimate of the radial and angular distributions of traps in the shell and of the average donor-trap distances. This analysis requires a comparison of time-resolved decay curves with theoretical curves derived from a reasonable physical model. In the following paper, we have calculated theoretical decay curves by means of computer-based simulations.[39] A comparison of theoretical data for model distributions with experimental fluorescence decays in water and in water-rich solvents indicate that the distribution of traps in the shell is strongly nonrandom. Advanced, i.e., fairly realistic and detailed, Monte Carlo simulations of chain conformations and the trap distribution in the shell for hydrophobically modified micelles are in progress, and results will be presented soon.

(4) Our study was directed toward understanding the behavior of modified copolymer micelles with end-capped polyelectrolytes blocks by hydrophobes. Since other workers have been considering adding "recognition elements" or "regulation elements" at the ends of corona of polymeric micelles for the purpose of directed drug delivery, our study may be relevant also for this important application if the recognition elements have some degree of hydrophobic character.[72−74]

**Acknowledgment.** This study was supported by the Grant Agency of the Czech Republic (Grant No. 203/01/0536) and by the Grant Agency of the Charles University (Grant No. 215/2000/BCh/Pr). S.E.W. would like to acknowledge support from the Robert A. Welch Foundation (Grant F-356).

## Appendix. Fluorometric Measurements in Tagged Micellar Systems

The emission intensity, $I_D^0$, of a donor D (excited at the wavelength $\lambda_D$ in the absence of energy traps and monitored at $\lambda_D^{em}$) is proportional to the intensity of the light, $I_D^{abs}$, absorbed by the donor D and to its fluorescence quantum yield, $\phi_D^0$, which reflects all processes that, in a given medium without energy traps, compete with the emission. The intensity, $I_D^{abs}$, is related to a proper value of the absorbance, $A_D(\lambda_D)$. However, the experimentally measured absorbance, $A_{exp}(\lambda_D)$, is due, in major part, to the inactive absorption by polymer backbone and to light scattering. Just a small part of the absorbed light (corresponding to $A_D(\lambda_D) = \epsilon_D(\lambda_D)c_D l$, where $\epsilon_D(\lambda_D)$ is the molar extinction coefficient of the donor, $c_D$ its molar concentration, and $l$ the optical path) is responsible for the excitation of donors. Absorption spectra of micellar solutions show that the inactive part represents almost 100% of the measured value and causes a strong attenuation of the excitation-active incident light. At low excitation intensity, the corrected fluorescence intensity is given by the following expression

$$I_D^0 \cong \phi_D^0 I_0^{cor}(\lambda_D) 10^{-A_{exp}(\lambda_D)} S_D(\lambda_D) 2.3\epsilon_D(\lambda_D) c_D l \quad \text{(A1)}$$

where $I_0^{cor}(\lambda)$ is the wavelength-corrected lamp intensity and the correction factor $S_D(\lambda_D)$ describes changes in the fluorophore (donor) properties after its attachment at the polymer chain and a possible energy transfer from the backbone to the pendant fluorophore. This term reflects the most unpleasant complication in the data treatment and evaluation of the transfer efficiency. The pertinent correction has to be investigated and assessed experimentally using the studied copolymers and model compounds.

As concerns the NRET from the excited donor D (naphthalene) to a trap T (anthracene), the light is absorbed by D under the same conditions as described above. A part of the photons, $(1 - \chi^{tr})$ is emitted at $(\lambda_D)^{em}$, while the other part, $\chi^{tr}$, is transferred to T. The sensitized T emission, $I_T^{sens}$, is controlled by the quantum yield of T and is affected by the microenvironment of T that may differ from that of D. Since the anthracene and naphthalene absorption partially overlap, the total anthracene emission intensity at $(\lambda_T)^{em}$ is a sum of two contributions.

$$I_T^{tot} \cong I_0^{cor}(\lambda_D)10^{-A_{exp}(\lambda_D)}[\chi^{tr}\phi_T{}^0 S_D(\lambda_D)2.3\epsilon_D(\lambda_D)c_D l + \phi_T S_T(\lambda_D)2.3\epsilon_T(\lambda_D)c_T l] \quad \text{(A2)}$$

The first term in the right-hand side of eq 2 describes the sensitized emission and the second describes the direct excitation contribution. The quantum yield $\phi_T$ of the trap, excited in a far blue-shifted region at $\lambda_D$, is not generally identical with $\phi^0{}_T$ that corresponds to $\lambda_T$. The most severe complications arise from the environment-sensitive shifts of the absorption bands between 250 and 300 nm and the changes in both $\epsilon_D$ and $\epsilon_T$ at the excitation wavelength, $\lambda_D$. Careful measurements with tagged copolymers and low-molar-mass model compounds allow for a reasonable correction of raw experimental data.

## References and Notes


(1) Riess, G.; Hurtres, G.; Bahadur, P. *Encyclopedia of Polymer Science and Engineering*, 2nd ed.; Wiley: New York, 1985; p 234.
(2) Tuzar, Z.; Kratochvíl, P. In *Surface and Colloid Science*; Matijevic, E., Ed.; Plenum Press: New York, 1993; Vol. 15, p 1.
(3) Almgren, M.; Brown, W.; Hvidt, S. *Colloid Polym. Sci.* **1995**, *273*, 2.
(4) Khougaz, K.; Astafieva, I.; Eisenberg, A. *Macromolecules* **1995**, *28*, 7135.
(5) Tuzar, Z. In *Solvents and Self-organization of Polymers*; Webber, S. E., Munk, P., Tuzar, Z., Eds.; NATO ASI Series E 327; Kluwer Academic Publishers: Dordrecht, The Netherlands, 1996; p 309.
(6) Tuzar, Z.; Pospíšil, H.; Pleštil, J.; Lowe, A. B.; Baines, L. B.; Billingham, N. C.; Armes, S. P. *Macromolecules* **1997**, *30*, 2509.
(7) Tsisilianis, C.; Voulgaris, D.; Štěpánek, M.; Podhájecká, K.; Procházka, K.; Tuzar, Z.; Brown, W. *Langmuir* **2000**, *16*, 6868.
(8) Procházka, K.; Martin, T. J.; Webber, S. E.; Munk, P. *Macromolecules* **1996**, *29*, 6526.
(9) Tuzar, Z. In *Solvents and Self-organization of Polymers*; Webber, S. E., Munk, P., Tuzar, Z., Eds.; NATO ASI Series E 327; Kluwer Academic Publishers: Dordrecht, The Netherlands, 1996; p 327.
(10) Tuzar, Z.; Webber, S. E.; Ramireddy, C.; Munk, P. *Polym. Prepr.* **1991**, *32* (1), 525.
(11) Munk, P. In *Solvents and Self-organization of Polymers*; Webber, S. E., Munk, P., Tuzar, Z., Eds.; NATO ASI Series E 327; Kluwer Academic Publishers: Dordrecht, The Netherlands, 1996; p 19.
(12) Wilhelm, M.; Zhao, C.-L.; Wang, Y.; Xu, R.; Winnik, M. A.; Mura, J.-L.; Riess, G.; Croucher, M. D. *Macromolecules* **1991**, *24*, 1033.
(13) Rager, T.; Meyer, W. H.; Wegner, G.; Winnik, M. A. *Macromolecules* **1997**, *30*, 4911.
(14) Astafieva, I.; Zhong, X. F.; Eisenberg, A. *Macromolecules* **1993**, *26*, 7339.
(15) Astafieva, I.; Khougaz, K.; Eisenberg, A. *Macromolecules* **1995**, *28*, 7127.
(16) Yu, Y. S.; Zhang, L. F.; Eisenberg, A. *Langmuir* **1997**, *13*, 2578.
(17) Zhang, L. F.; Eisenberg, A. *Macromolecules* **1999**, *32*, 2239.
(18) Shen, H. W.; Zhang, L. F.; Eisenberg, A. *J. Am. Chem. Soc.* **1999**, *121*, 2728.
(19) Shen, H. W.; Eisenberg, A. *J. Phys. Chem. B* **1999**, *103*, 9473.
(20) Shen, W. H.; Eisenberg, A. *Macromolecules* **2000**, *33*, 2561.
(21) Antonietti, M.; Heinz, S.; Schmidt, M.; Rosenauer, C. *Macromolecules* **1994**, *27*, 3276.
(22) Antonietti, M.; Förster, S.; Östrich, S. *Macromol. Symp.* **1997**, *121*, 75.
(23) Regenbrecht, M.; Akari, S.; Förster, S.; Mohwald, H. *J. Phys. Chem. B* **1999**, *103*, 6669.
(24) Buthun, V.; Lowe, A. B.; Billingham, N. C.; Armes, S. P. *J. Am. Chem. Soc.* **1999**, *121*, 4288.
(25) Lee, A. S.; Gast, A. P.; Buthun, V.; Armes, S. P. *Macromolecules* **1999**, *32*, 4302.
(26) Wooley, K. L. *J. Polym. Sci.* **2000**, *38*, 1397.
(27) Munk, P.; Procházka, K.; Tuzar, Z.; Webber, S. E. *CHEMTECH* **1998**, *28* (10), 20.
(28) Kiserow, D.; Procházka, K.; Ramireddy, C.; Tuzar, Z.; Munk, P.; Webber, S. E. *Macromolecules* **1992**, *25*, 461.
(29) Tuzar, Z.; Kratochvíl, P.; Procházka, K.; Munk, P. *Collect. Czech. Chem. Commun.* **1993**, *58*, 2362.
(30) Tuzar, Z.; Procházka, K.; Zusková, I.; Munk, P. *Polym. Prepr.* **1993**, *34* (1), 1038.
(31) Tian, M.; Quin, A.; Ramireddy, C.; Webber, S. E.; Munk, P.; Tuzar, Z.; Procházka, K. *Langmuir* **1993**, *9*, 1741.
(32) Teng, Y.; Morrison, M.; Munk, P.; Webber, S. E.; Procházka, K. *Macromolecules* **1998**, *31*, 3578.
(33) Štěpánek, M.; Krijtová, K.; Limpouchová, Z.; Procházka, K.; Teng, Y.; Webber, S. E.; Munk, P. *Acta Polym.* **1998**, *49*, 96; **1998**, *49*, 103.
(34) Procházka, K.; Martin, T. J.; Munk, P.; Webber, S. E. *Macromolecules* **1996**, *29*, 6518.
(35) Štěpánek, M.; Procházka, K. *Langmuir* **1999**, *15*, 8800.
(36) Štěpánek, M.; Procházka, K.; Brown, W. *Langmuir* **2000**, *16*, 2502.
(37) Procházka, K.; Kiserow, D.; Ramireddy, C.; Tuzar, Z.; Munk, P.; Webber, S. E. *Macromolecules* **1992**, *25*, 454.
(38) Ramireddy, C.; Tuzar, Z.; Procházka, K.; Webber, S. E.; Munk, P. *Macromolecules* **1992**, *25*, 2541.
(39) Uhlík, F.; Limpouchová, Z.; Matějíček, P.; Procházka, K.; Tuzar, Z.; Webber, S. E. *Macromolecules* **2002**, *35*, 9497.
(40) Kratochvíl, P. In *Classical Light Scattering from Polymer Solutions, Polymer Science Library 5*; Jennkins, A. D., Ed.; Elsevier: Amsterodam, 1987.
(41) Tuzar, Z.; Kratochvíl, P. *Collect. Czech. Chem. Commun.* **1967**, *32*, 3358.
(42) Jakeš, J. *Czech. J. Phys.* **1988**, *B38*, 1305.
(43) Förster, T. *Discuss. Faraday Soc.* **1959**, *7*, 27.
(44) Berleman, I. B. *Energy Transfer Parameters of Aromatic Compounds*; Academic Press: New York, London, 1973.
(45) Holden, D. A.; Guillet, J. E. *Macromolecules* **1980**, *13*, 289.
(46) Liu, G.; Guillet, J. E.; Al-Takrity, T. B.; Jenkins, A. D.; Walton, D. R. M. *Macromolecules* **1991**, *24*, 68.
(47) Martin, T. J.; Webber, S. E. *Macromolecules* **1995**, *28*, 8845.
(48) Katchalski, A. *J. Polym. Sci.* **1951**, *7*, 393.
(49) Arnold, R. *J. Colloid Sci.* **1957**, *1*, 549.
(50) Anufrieva, E. V.; Birshtein, T. M.; Nekrasova, T. N.; Ptitsyn, C. B.; Scheveleva, T. V. *J. Polym. Sci., Part C* **1968**, *16*, 3519.
(51) Delben, F.; Crezcenzi, V.; Quadrifoglio, F. *Eur. Polym. J.* **1972**, *8*, 933.
(52) Koenig, J. L.; Angood, A. C.; Semen, J.; Lando, J. B. *J. Am. Chem. Soc.* **1969**, *91*, 7250.
(53) Wang, Y.; Morawetz, H. *Macromolecules* **1986**, *19*, 1925.
(54) Bednář, B.; Trněná, J.; Svoboda, P.; Vajda, S.; Fidler, V.; Procházka, K. *Macromolecules* **1991**, *24*, 2054.
(55) Soutar, I.; Swanson, L. *Macromolecules* **1994**, *27*, 4304.
(56) Lyatsaya, Yu. V.; Leermakers, F. M. A.; Fleer, G. J.; Zhulina, E. B.; Birstein, T. M. *Macromolecules* **1995**, *28*, 3562.
(57) ten Brinke, G.; Hadziioanou, G. *Macromolecules* **1987**, *20*, 486.

(58) Tuzar, Z.; Koňák, Č.; Štěpánek, P.; Pleštil, J.; Kratochvíl, P.; Procházka, K. *Polymer* **1990**, *31*, 2118.
(59) Balsara, N. P.; Tirrel, M.; Lodge, T. P. *Macromolecules* **1991**, *24*, 1975.
(60) Zhou, Z.; Chu, B.; Pfeiffer, D. G. *Langmuir* **1995**, *11*, 1956.
(61) Saito, R.; Yoshida, S.; Ishusu, K. *J. Appl. Polym. Sci.* **1997**, *63*, 849.
(62) Chu, B.; Zhou, Z. K.; Liu, T. B.; Wu, C. H. *Macromol. Symp.* **1997**, *118*, 221.
(63) Koňák, Č.; Fleischer, G.; Tuzar, Z.; Bansil, R. *J. Polym. Sci. B* **2000**, *38*, 1312.
(64) Unali, G. F.; Armes, S. P.; Billingham, N. C.; Tuzar, Z.; Hamley, I. W. *Polym. Prepr.* **1999**, *40* (2), 259.
(65) Raspaud, E.; Lairez, D.; Adam. M.; Carton, J.-L. *Macromolecules* **1994**, *27*, 2956.
(66) Semenov, A. N.; Joanny, J.-F.; Khokhov, A. R. *Macromolecules* **1995**, *28*, 1066.
(67) Xing, L.; Mattice, W. L. *Macromolecules* **1997**, *30*, 1711.
(68) Xing, L.; Mattice, W. L. *Macromol. Theory Simul.* **1997**, *6*, 553.
(69) Susharina, N. P.; Linse, P. *Eur. Phys. J.* **2000**, *52*, 151.
(70) Nagarajan, R.; Ganesh, K. *J. Chem. Phys.* **1989**, *90*, 5843.
(71) Matějíček, P.; Limpouchová, Z.; Uhlík, F.; Procházka, K.; Tuzar, Z.; Webber, S. E. *Collect. Czech. Chem. Commun.* **2002**, *67*, 531.
(72) Kataoka, K.; Harashima, H. *Adv. Drug Delivery Rev.* **2001**, *52*, 151.
(73) Yamamoto, Y.; Nagasaki, Y.; Kato, Y.; Sugiyama, Y.; Kataoka, K. *J. Controlled Release* **2001**, *77*, 27.
(74) Nagasaki, Y.; Yasugi, K.; Yamamoto, Y.; Harada, A.; Kataoka, K.*Biomacromolecules* **2001**, *2*, 1067.

MA012074G